Journal Name

ARTICLE TYPE

Cite this: DOI: 10.1039/xxxxxxxxxx

Self-assembly of bis-salphen compounds: from semi-flexible chains to webs of nanorings†

Sergey V. Pyrlin*[a], Nicholas D.M. Hine[b], Arjan W. Kleij[c,d] and Marta M.D. Ramos*[a]

Received Date
Accepted Date

DOI: 10.1039/xxxxxxxxxx

www.rsc.org/journalname

The recently-observed self-assembly of certain salphen-based compounds into neuron-like networks of microrings interconnected with nano-thin strings may suggest a new highly-potent tool for nanoscale patterning. However, the mechanism behind such phenomena needs to be clarified before they can be applied in materials design. Here we show that, in contrast with what was initially presumed, the emergence of a "rings-and-rods" pattern is unlikely to be explained by merging, collapse and piercing of vesicles as in previously reported cases of nanorings self-assembly via non-bonding interactions. We propose an alternative explanation: the compounds under study form a 1D coordination polymer, the fibres of which are elastic enough to fold into toroidal globules upon solvent evaporation, while being able to link separate chains into extended networks. This becomes possible because the structure of the compound's scaffold is found to adopt a very different conformation from that inferred in the original work. Based on *ab initio* and molecular dynamics calculations we propose a step-by-step description of self-assembly process of a supramolecular structure which explains all the observed phenomena in a simple and clear way. The individual roles of the compound's scaffold structure, coordination centres, functional groups and solvent effects are also explained, opening a route to control the morphology of self-assembled networks and to synthesize new compounds exhibiting similar behaviour.

Introduction

In an ancient legend, queen Dido was promised as much land as she could enclose with one bull's skin, so she tore it into fine strips, made a thong and laid out a circular arc with it, the internal area of which was sufficient to build the whole city of Carthage. The problem of enclosing the maximum area within a fixed boundary is referred to as the "Dido Problem".[1] In modern materials engineering, the formation of micro- and nano-rings finds application within many fields, including catalysis and opto-electronic devices. In both cases one seeks to maximise the area of pores in a functional coating for best permeability or transparency, while maintaining the connectivity of the coating material for optimal strength and electronic conductivity.[2–6]

In the "top-down" approach circular patterns are routinely formed using capillary effects in evaporating solvent: solute molecules agglomerate either along droplet periphery ("coffee-ring effect",[2,3] figure 1a) or around the spontaneous opening in thinning liquid film ("pinhole opening",[7,8] figure 1b), dragged by the solvent flow, caused by faster evaporation at the curved surface of the dewetting rim. The "openings" in liquid film can also be initiated deliberately by condensing vapour droplets onto it to fabricate regular honeycomb-like networks ("breath figure" method, figure 1c).[4,9]

The "bottom-up" approach, on the other hand, relies on the interplay between solute-solute and solute-solvent interactions. The most common way is aggregation of amphiphilic molecules into hollow-core vesicles or micrometer-long cylindrical or "worm-like" micelles.[10–14] As a special case, ring-like (or toroidal) micelles can form from both types of aggregates either by closing end-points of a worm-like micelle(figure 1e),[15–18] or

[a] *Department of Physics and Center of Physics, University of Minho, Campus de Gualtar, Braga 4710 - 057, Portugal; E-mail: pyrlinsv@fisica.uminho.pt, marta@fisica.uminho.pt*
[b] *Department of Physics, University of Warwick, Coventry CV4 7AL, UK*
[c] *Institute of Chemical Research of Catalonia (ICIQ), the Barcelona Institute of Science and Technology, Av. Països Catalans 16, Tarragona 43007, Spain*
[d] *Catalan Institute of Research and Advanced Studies (ICREA), Pg. Lluis Companys 23, Barcelona 08010, Spain*

† Electronic Supplementary Information (ESI) available: further discussion and computational details, figures S1-S6 and table S1. See DOI: 10.1039/b000000x/

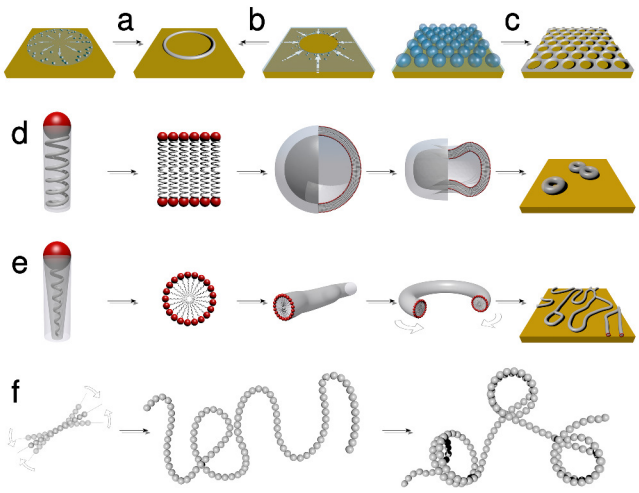

Fig. 1 Schematic representation of possible mechanisms of ring-like and network structures formation: "coffee-ring" effect (a), "pinhole opening" (b), "breath figure" method (c), assembly of amphiphilic molecules into collapsing vesicles (d), worm-like micelles and their networks (e) and polymer coil to toroidal globule transition (f); white arrows indicate the direction of particles' spontaneous movement due to either solvent drag (a,b), surface energy minimization (e) or polymer chain elasticity (f)

by piercing of a deflating vesicle as solvent evaporates (figure 1d).[15,19]

Another phenomenon leading to the formation of molecular rings is the "coil-to-toroidal globule" transition,[20–24] observed previously for isolated chains of "semiflexible" polymers, such as DNA,[25] xanthan[26] among others. Chains of such polymers stay rigid at the nanometre level, but are flexible at a larger scale.[22] As the solvent evaporates or is replaced by "poorer" solvent, i.e. the one in which polymer-solvent interactions are weaker,[27], such chains may assume a ring-like shape resulting from the competition between the attraction of chain segments and their elasticity, preventing the chains from bending below certain curvature (figure 1f). As a special case, when the solvent evaporation rate prevents coil relaxation to a single globule, a collection of a few rings, connected with a single molecule-wide string, can be observed.[28,29] However, these polymer chains are inherently limited in size, so no extended network-like structures were observed so far.

The recently observed[30] ability of zinc-centred phenyl functionalized symmetrical salphen-based complexes (figure 2a) to form molecular networks (figure 2b) clearly differs from the previously observed cases not only because of the unusual size of self-assembled rings (average diameter $\sim 2\,\mu$m, compared to few hundreds of nanometres typical for toroidal micelles),[15–19] but also due to their well defined neuron-like pattern of multiple ~ 100 nm thick rod-like connections. Such pattern is very distinct from honeycomb lattice of "breath figure" method or from networks of randomly oriented and mostly winding "worm-like" micelles,[31,32] where ring attached to a string can only occasionally be observed.[17,31] Furthermore, this unusual self-assembly was also demonstrated inside a polymer matrix, in contrast to the other methods which only produced rings or networks on substrate surfaces.

Self-assembly of similar metal-organic complexes has been very actively studied during recent decades and is known to result from the balance of non-bonding attraction (from cation-oxygen, cation-π,$\pi-\pi$ or hydrogen interactions) and steric repulsion.[33–36] Controlling the molecular structure of organic ligands, a variety of nanoscale supramolecular assemblies were demonstrated feasible including dimers,[37,38] cage-like aggregates[39,40] and even rings consisting of 5-30 porphyrin bases.[41] However, on the larger scale ($\gtrsim 0.1\,\mu$m) collections of rigid fibrils,[42] branched nanogels[43–45] or crystals[46–49] were obtained, even when the bis-salphen compounds quite similar to the one shown in figure 2a were studied.[47,50] The network of rings and rods remains so far a unique such observation.[30] It is, therefore, important to study this self-assembly phenomenon at the molecular level as it will help to understand how the chemical structure of this particular compound translates into formation of this pattern and, ultimately, to control the morphology of such networks.

By analogy with previously reported cases of toroid self-assembly, Escárcega-Bobadilla *et al.*[30] suggested that the rings may form from deflating vesicles, which also shrink during solvent evaporation, leaving rod-like connections extruded from the points of contact between neighbouring vesicles (figure S1 in the Electronic Supplementary Information (ESI)). This hypothesis, although seemingly viable, raises more questions than it tries to answer: given the reported average diameter of the rings, self-assembled from bis-Zn(salphen) complexes, $\sim 2.1\,\mu$m and thickness of their rims and connecting rods $\sim 0.14\,\mu$m it is easy to estimate (see section S1 of Supplementary Information) that if the average rod length is equal to the ring diameter the initial vesicle should be at least $\sim 3\,\mu$m in diameter and have a thickness at most ~ 5 nm. This already puts such hypothetical vesicles in the range of giant unilamellar vesicles,[51,52] which usually require certain treatment to fabricate, and makes the formation of longer rods (up to 15 μm[30]) quite questionable. Furthermore, it is unclear why the symmetric complex shown in figure 2a would form vesicles and what causes such significant shrinkage. Vesicles of metal-organic compounds were already observed,[19] however these compounds were specifically functionalized to give them amphiphilic abilities. Clusters of partially merging vesicles have also been reported before,[19,53] however toroidal micelles forming form such vesicles remained fused with no rods extruded.

In this article we employ all-atom molecular dynamics (MD) modelling to explore the conformational space of phenyl-functionalized bis-Zn(salphen) complexes, details of their interaction with solvent and possible patterns of their self-assembly. We demonstrate that the formation of "rings-and-rods" networks has in fact many similarities to the aforementioned "coil-toroidal globule" transition rather than vesicle deflation. Based on our simulations we pinpoint a specific path through which such compounds can form the micro-scale structures observed previously.[30] We have also examined mechanical properties of these macromolecular structures and estimated the free energy gains associated with different steps of the proposed mechanism using the umbrella sampling (US) and free energy perturbation (FEP) methods. These calculations help to explain how a particular sol-

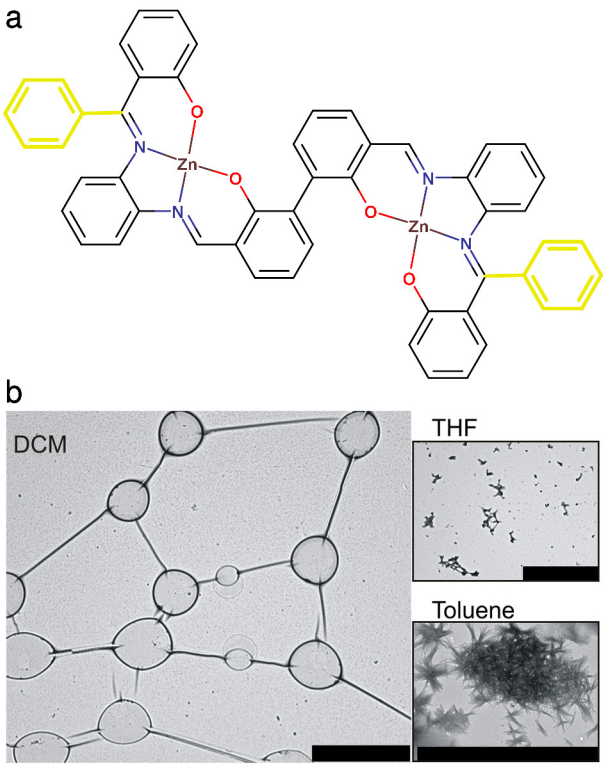

Fig. 2 Schematic representation of bis-Zn(salphen) complex (top, yellow hexagons highlight the key phenyl substituents) and self-assembled structures, obtained by drop-casting bis-Zn(salphen) complexes from various solvents[30] (bottom, the scale bars indicate 5 μm)

vent affects the growth of self-assembled aggregates determining the shape and size of the resulting structure.

Results and discussion

MD studies of bis-Zn(salphen) complexes: possible conformations and behaviour in solvent

Several unexplained observations[30] may hint to the nature of this phenomenon. The desired networks were only obtained by deposition of phenyl-functionalized complexes from dichloromethane (DCM). Replacement of phenyl side-groups by methyl-termination (figures S2a,b) resulted in disconnected drops, while drop-casting from other solvents produced only short fibres (tetrahydrofuran, THF) or needle-like nanocrystals (toluene) (figure 2b). Motivated by these striking differences, we have conducted all-atom molecular dynamics simulations of bis-Zn(salphen) complexes both in vacuum and selected solvents to explore the rationale behind such behaviour. Details of the chosen parametrization and simulations procedures can be found in the Methods section. Validation of the chosen parametrization against *ab initio* calculations are discussed in section S3 in the ESI.

The first feature of the complex (figure 2a) setting it apart from similar Zn complexes studied before, including very similar complexes,[47,50] is the presence of several flexible joints allowing it to have a number of conformers. Due to the relative rigidity of the N_2O_2 coordination around the Zn centres, the conformational space of the molecule can be reduced to the two dihedral angles[54], Θ and Φ as shown in figure 3a. From the corresponding free energy profiles (figure 3b,c), calculated in vacuum using the umbrella sampling method (US),[55] it follows that the most thermodynamically stable conformation of the complex is the "closed" ($\Theta \sim 50^\circ$ or $\Theta \sim 250^\circ$) *W*-shaped geometry (side-groups point to the same side, $\Phi \sim -80^\circ$), in which the two cations participate in the formation of Zn_2O_2-square unit, seen in mono-salphen dimers.[34,38] However, association into any extended supramolecular structure requires climbing $\sim 5-6$ kcal/mol barrier to reach a meta-stable "open" conformation ($\Theta \sim 150^\circ$).

Another distinct conformation can be achieved, if one of the side-groups is rotated to the other side of the molecule ($\Phi \sim 50^\circ$) and the bis-Zn(salphen) complex assumes an *S*-like shape. This only requires crossing a narrow $\sim 6-7$ kcal/mol barrier and the free energy difference between the valleys is quite small so both conformers should coexist in solution (figure 3e). Just like in the case of the *W*-shaped geometry, the *S*-like conformation can exist both in "open" and "closed" form with the only difference that the corresponding free energy profile is now symmetric. As we will show later, the difference between *W*- and *S*-like conformations is crucial when discussing supramolecular association of the bis-salphen complexes.

However, the relative stability of these conformations can be altered due to strong interactions with solvent molecules, seen by a high peaks of the corresponding radial distribution function $g(r)$ (figure S3 in the ESI). Strong electrostatic attraction between the zinc cation and oxygen atom of THF molecule, reflecting the known behaviour of zinc based complexes in coordinating solvent such as THF or pyridine,[36,44] decreases the stability of Zn_2O_2-square units in this solvent, making the "open" geometry more stable. A similar, though much weaker effect occurs in toluene due to cation-π and $\pi-\pi$ interactions. In DCM, on the other hand, the "closed" conformation remains dominant.

One consequence of the solvent-induced conformational change is a marked difference in diffusion speed, which affects the rate at which self-assembled structures grow.[56] Translational diffusion coefficients of single bis-Zn(salphen) complexes, estimated numerically from the set of 40 independent trajectories in explicit solvent[57], show almost twice as fast diffusion rates in DCM: 730 $\mu m^2/s$ compared to 390 $\mu m^2/s$ in THF and 420 $\mu m^2/s$ in toluene (estimated error $\leq 10\ \mu m^2/s$) in contrast with the Stokes-Einstein relation[58] predicting a ratio of $1 : 0.9 : 0.73$ if solely the viscosity of the solvent would matter. These numerical estimates are comparable with the experimentally measured diffusion rate of $540\ \mu m^2/s$ for the smallest associates in DCM.[30] As we will show later, this observation most likely correspond to dimers of complexes under study, so somewhat lower value is expected. The observed difference should, apart from the viscosity of the solvent, arise from the dominance of "closed" conformations in DCM (smaller radius of gyration) and zinc-solvent interactions in THF and TOL and should contribute to the smaller size of aggregates observed in the latter two solvents compared to DCM alongside with free energy of binding, that will be discussed later.

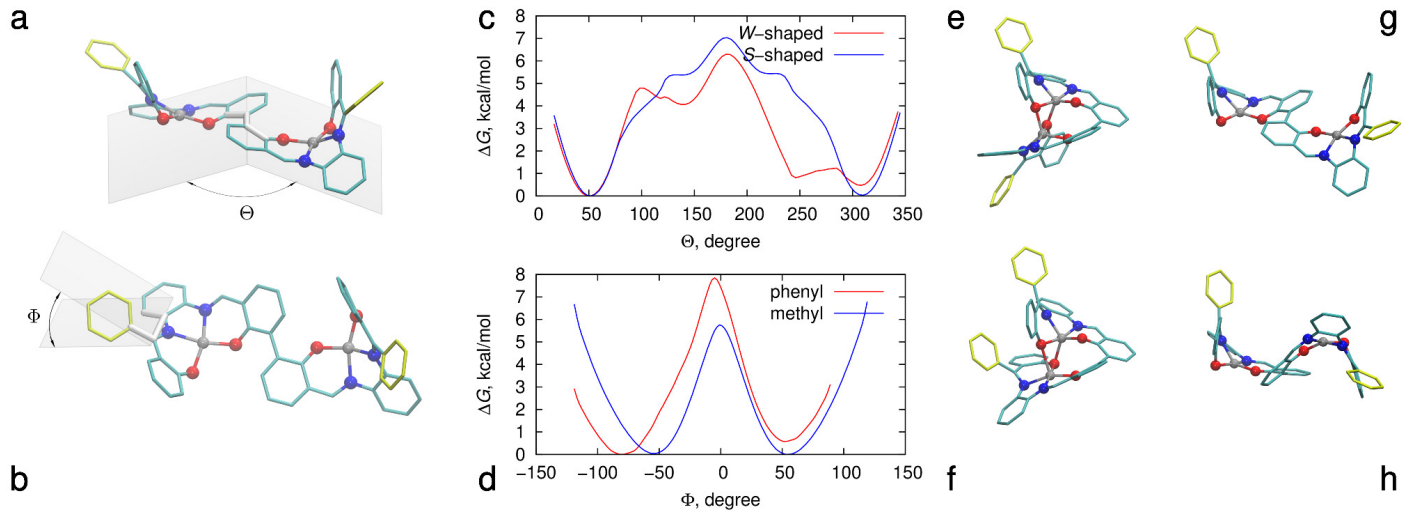

Fig. 3 Possible conformations of structures of the bis-Zn(salphen) complex: definition of conformational coordinate angles Θ (a) and Φ (b), white tubes highlight the corresponding dihedral; free energy profiles from US calculations in vacuum, corresponding to Θ(c) and Φ(d) angles; *W*-like (e,g) and *S*-like (f,h) conformations correspondingly in "closed" (e,f) and "open" (g,h) forms

Table 1 Geometry parameters of idealized periodic structures

$\alpha-$ *structure*			
$\tilde{t}$, (nm)	(0.01,	0.00,	0.41)
$\tilde{OO'}$	(-0.10,	-0.07,	0.94)
δ			-11.72°
$\beta-$ *structure*			
$\tilde{a}$, (nm)	(2.00,	0.00,	0.00)
$\tilde{b}$, (nm)	(2.40,	0.92,	0.02)
$\tilde{a}'$, (nm)	(3.99,	0.00,	0.00)
$\tilde{b}'$, (nm)	(0.00,	2.00,	0.00)
$\tilde{c}'$, (nm)	(0.00,	0.35,	1.10)

Alternative patterns of supramolecular association and chain elasticity

Based on the observations made in the previous section we have identified two ways in which long periodic structures can be formed from bis-Zn(salphen) complexes (figure 4a,d). The parameters used to create the initial structures corresponding to single periodic chains and multiple chain arrangements were determined from optimisation of the selected idealized fragments in vacuum and are reported in the Table 1. To investigate if any of these arrangements can explain the observed phenomena we have studied the behaviour of such chains of up to 8 periodic units (contour length ~8 nm) in explicit solvent during intervals of up to 5 ns, monitoring their structure.

Initially,[30] the rings and rods were considered to be formed by *W*-shaped conformers of bis-Zn(salphen) complexes in a stack-like arrangement (hereafter called *"alpha"* or α, figure 4a) inspired by the crystal structure of the unsubstituted ligand (figures S2c,d). This structure can be reproduced by repetitive displacement of a *W*-shaped conformation in the "open" state by the vector $\vec{t}$, almost parallel to the local z-axis, and rotation by the angle δ around the axis OO' as shown in figure 4a (local x-axis is chosen along the central C-C bond, while y-axis goes in the direction of a vector connecting cations). Such chains make a full turn in approximately 38 units, covering the distance $T = 14.5$ nm, and can be paired with a second chain, rotated 180° around the axis of the helix. However, our current simulations show that such an arrangement, although stable in vacuum and expected to be quite rigid, becomes quite fragile against torsional deformations in explicit solvent: accidental displacement can switch one of the Zn-O bonds to form a stronger Zn_2O_2-square unit with just one of the neighbouring complexes. This results in breaking of the initial chain into dimers or trimers already after ~0.5 ns, independently of the solvent as can be seen from the distortion of the cation pair distribution function (figure 4b). Therefore, long chains having such a geometry are unlikely to form in solvent and cannot explain the observed phenomena.

However, *S*-like conformers of the same bis-Zn(salphen) complexes can link via Zn_2O_2 units into linear chains (hereafter referred to as *"beta"* or β, figure 4d), which remain stable both in vacuum and solvent due to the combination of strong Zn_2O_2 links and flexibility of rotation around the central bonds, as can be seen from well-resolved peaks of the zinc pair distribution function close to their initial positions (figure 4e). Small displacement of the peaks towards smaller Zn-Zn distances can be noticed as the result of local bending of single chains during simulation.

The stretched-aside phenyl groups can link such chains via $\pi-\pi$ or cation-π interactions into thicker fibres or even in layered structure as shown in the figure 4d. This concatenation of linear chains into regular planar structures via side-groups interactions is similar to β-sheet formation commonly observed for certain proteins.[59–61] The dimers along Zn-O bonded chains are not exactly equivalent: there is a small alternating rotation between direct neighbours and therefore the primitive cell of such 2D sheet (designated with the vectors $\vec{a}$ and $\vec{b}$) consists of two of such dimers. However it is more convenient to work with a rectangular four-dimer supercell designated with the vectors $\vec{a}'$ and $\vec{b}'$. The sheets can be stacked together along the $\vec{c}'$ vector into a layered crystal structure (Table 1).

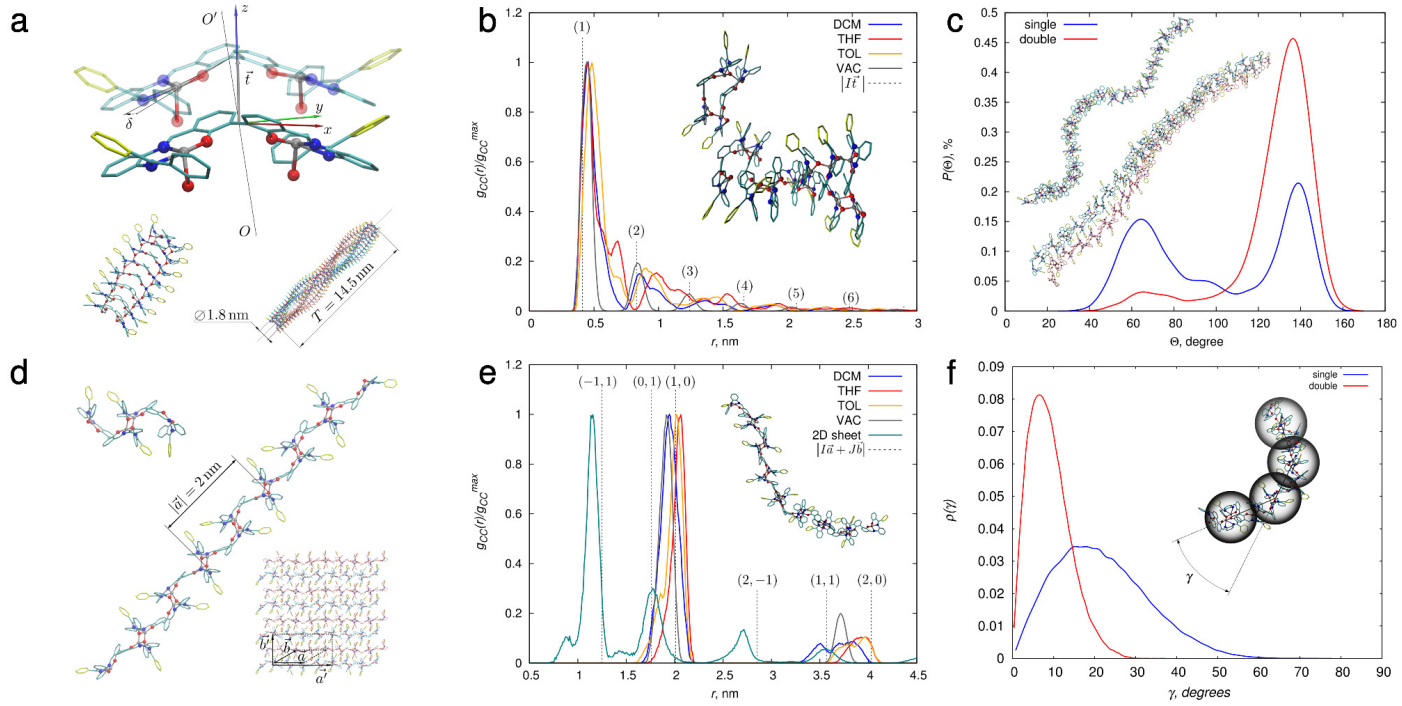

Fig. 4 Comparison of the possible polymeric chains structures, corresponding to *W*- and *S*-shaped conformers: (a) and (d)- geometries of periodic transition of $\alpha-$ and $\beta-$chains and fragments of corresponding single and multiple chain structures, (b) and (e) - corresponding profiles of radial pair distribution function of Zn cations in vacuum and the three selected solvents, including the expected positions of peaks for idealized structures, (c) - distribution of Θ-angles, samples for single and double $\beta-$chains with N=16 periodic units over 40 ns long simulation in vacuum, (f) - corresponding distributions of angles between dimer-dimer bonds

To study the effect of such binding on the elasticity of the self-assembled chains we have monitored the folding of single- and $\pi-\pi$ bonded double-stranded chains of up to 16 periodic units (contour length ~30 nm) during a 40 ns time under Langevin thermostat[62] without explicit solvent. Across 5 independent trajectories for each case we have collected the distribution of Θ angles in both types of chains and corresponding angles between periodic units along the chain (γ) as shown in figure 4c,f. Interestingly, a drastic change of behaviour is observed: while single chains show a significant flexibility with γ angles reaching up to $\sim 60^\circ$ originating from a large proportion of folded bis-salphen compounds as indicated by the lower peak of Θ distribution, a double chain is already relatively rigid. The $\pi-\pi$ binding of the two chains together significantly reduces folding of the central dihedrals of bis-salphen compounds, resulting in much narrower γ-distribution and, therefore, in more elastic behaviour. This is especially noteworthy regarding the fact that similar bis-Zn(salphen) complexes do not form networks, if phenyl groups are substituted by methyl groups,[30] collapsing then into isolated spherical droplets like typical flexible polymers.[63]

Proposed mechanism of self-assembly and free energy calculations

Based on the observations above, we propose the following steps (figure 5) of bis-Zn(salphen) polymeric chain self-assembly responsible for the formation of "rings-and-rods" network. We have estimated the effect of solvent by calculating the free energy changes corresponding to the outlined transitions in the three selected solvents using the "alchemical transformations" approach combined with the free energy perturbation (FEP) method.[64] Within this approach (figure 6), instead of directly simulating dissociation of the molecular clusters in solvent under external force, causing an abrupt shift of the potential of mean force with increasing distance, the transformation was split in the two separate processes. These processes are dissociation in vacuum and solution of both initial and final molecular structures in the selected solvent. Within this approach the potential energy of the two component system is split into the following contributions:

$$U_{12} = U_1 + U_2 + \lambda_{vdW} U_{12}^{vdW} + \lambda_{Coul} U_{12}^{Coul}; \qquad (1)$$

where $U_{1(2)}$ is the internal energy of each of the first (or second) subsystems, while U_{12}^{vdW} and U_{12}^{Coul} - are correspondingly the energies of van der Waals and electrostatic interactions between the subsystems. Each process is simulated by scaling the coupling parameters λ associated with van der Waals (λ_{vdW}) and electrostatic (λ_{Coul}) interactions between the two subsystems to be decoupled: complex-complex for dissociation and complex-solvent for solution.

The free energy of a transformation in solvent ($\Delta G^S_{R\to P}$, where *S* refers to DCM, THF or toluene) can then be estimated as:

$$\Delta G^S_{R\to P} = \Delta G^P_{V\to S} - \Delta G^R_{V\to S} + \Delta G^V_{R\to P}; \qquad (2)$$

where $\Delta G^V_{R\to P}$ is the free energy change of the corresponding

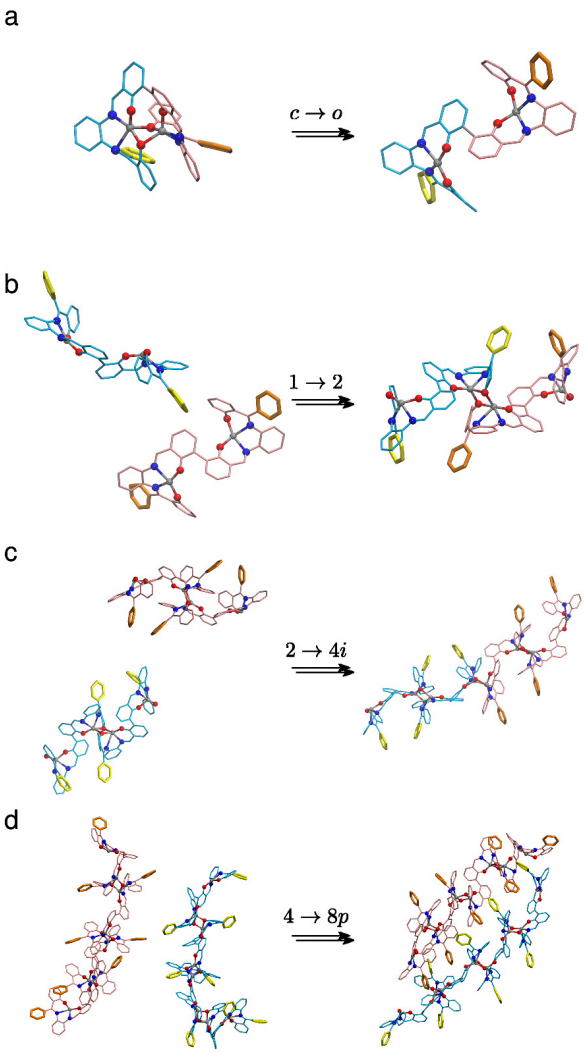

Fig. 5 Stages of bis-Zn(salphen) chain self-assembly: "openning" of isolated "closed" complex (a) Zn-O guided assembly of dimer (b) and tetrameric chain (c) and $\pi-\pi$ binding of two chains (d)

transformation in vacuum and $\Delta G^{R(P)}_{V\to S}$ is the solution free energy of the reactants (or the products). The latter term was estimated as negative of the free energy change during decoupling the supramolecular system of bis-Zn(salphen) complexes in the desired conformation from solvent. Subsequent dissociation of multi-molecular systems in vacuum was modelled in a similar way scaling down the interactions between dissociating parts. For single complex "opening" the value of 5.4 ± 0.1 kcal/mol was used for $\Delta G^{V}_{R\to P}$ as follows from earlier US calculations. The free energy of solution of single complexes and dimers from the previous calculations were reused for estimation of the association energies of the corresponding higher-order structures.

The resulting estimates are summarised in table 2. As is commonly used, a negative sign means that the final product (P) of the transition is thermodynamically more favoured than the initial reactant (R), therefore the $R\to P$ transition occurs spontaneously.

In the first step of the proposed self-assembly process, single

Table 2 Free energies of transitions in solvent from FEP calculations (confidence interval with 95% probability)

	$\Delta G^{S}_{R\to P}$ (kcal/mol)		
Transition	DCM	THF	Toluene
$c\to o$	5.2±0.6	-5.6±0.6	3.7±1.4
$1\to 2$	-8.6±1.6	-9.9±1.4	-13.1±1.9
$2\to 4i$	-18.0±3.5	-5.4±2.3	-14.7±1.6
$4\to 8p$	-5.1±1.4	-13.3±11.2	-15.9±3.8

complexes join into dimers through strong Zn-O interactions between one of the two metal centres from each molecule (figure 5a). This transition is strongly favourable in all the three solvents, which is indicated by large negative values of $\Delta G^{S}_{1\to 2}$ in the Table 2. Such a dimer has a diameter of ~ 2 nm and corresponds to the smallest associates (19.68 Å) observed in DCM.[30] Dimerization occurs even despite the aforementioned difference in preferred conformations of stand-alone molecules. This is also indicated by the different sign of $\Delta G^{S}_{c\to o}$, corresponding to "opening" transition. This occurs as the formation of inter-molecular zinc-oxygen bonds weakens the coordination interaction between the halves of the same complex, holding it "closed".

Such dimers serve as the primary building blocks for the higher order supramolecular structure. Contrary to what was initially implied,[30] here we suggest that both Zn-O and $\pi-\pi$ interactions are equally important for the self-assembly process. The former is stronger at first, promoting linear growth of supramolecular chains (figure 5b). However, as chains grow longer, the probability that the endpoints of long chains will meet decreases. Conversely, the importance of the $\pi-\pi$ bonding increases proportionally to the chain length (figure 5c), leading to joining of the individual chains into thicker, longer and more rigid fibres.

At this stage the effect of solvent becomes determining as shown by the ratio between free energy gain corresponding to binding of two dimers into tetrameric chains via coordination interaction ($\Delta G_{2\to 4i}$) and entangling of two tetramer segments of periodic chains into double chains via $\pi-\pi$ and cation-π interactions ($\Delta G_{4\to 8p}$). It becomes clear that DCM favours association of zinc complexes via Zn-O bonding. At the same time interactions via side-groups is the least favourable in DCM, which can be attributed to the size of solvent molecules. Smaller-sized DCM molecules can penetrate the gaps between the two associated chains more easily, disrupting weak $\pi-\pi$ interactions and promoting the formation of long flexible chains that aggregate into thicker fibres only at a late stage of solvent evaporation.

On the contrary, strong interactions between zinc ions and oxygen atoms of THF molecules makes concatenation of dimers via coordination bonding far less favourable, similar to the effect of adding pyridine to other zinc-substituted compounds.[42] In toluene, on the other hand, the free energy gain from the two binding types of the associated Zn(salphen) complexes become comparable already for very short chains, promoting formation of sheet-like structures.

Relatively large deviations of the estimated free energy gains are explained by high flexibility of the chains in the explicit solvent. Results for $\pi-\pi$ bonded chains, especially in case of THF, are particularly sensitive to this as small displacements can cause

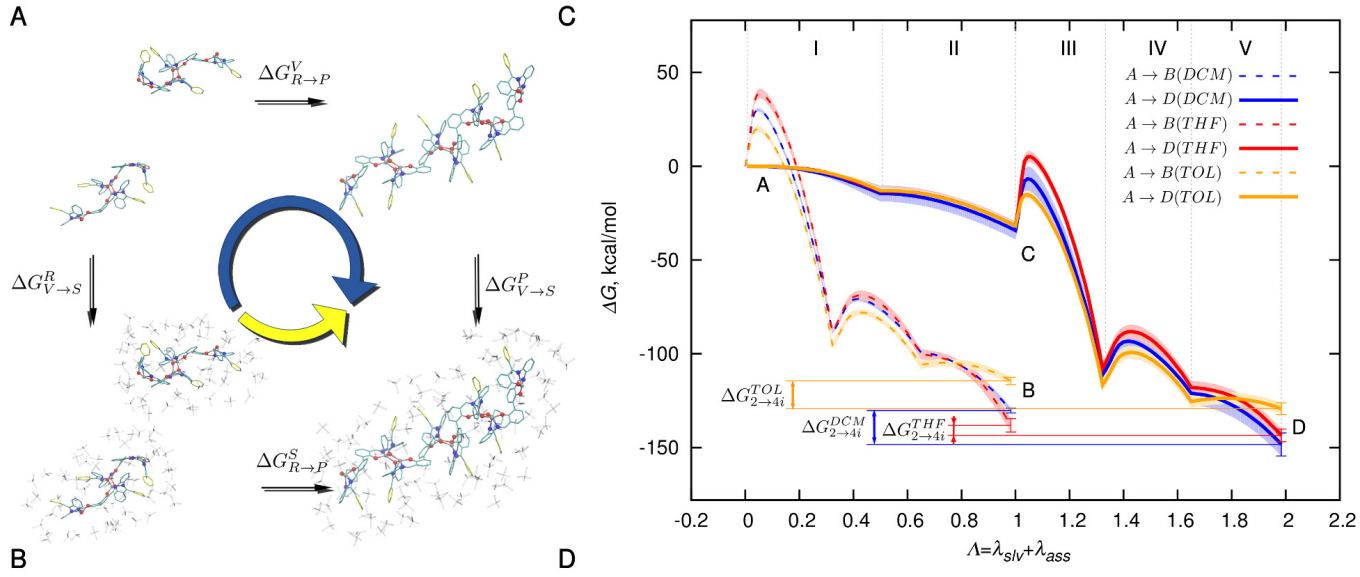

Fig. 6 Estimation of association binding energies in solvent via "alchemical transformation" approach: (a) - the thermodynamic cycle corresponding to the simulation process, (b) - free energy change along the path of simulation. The solid curves show the averages between 3 independant simulations, while the shaded areas and bars indicate estimated errors. All curves are superimposed so that they start from the state A, which is the common point for the two pathways, the simulations go in the opposite direction ($D\to C\to A$ and $B\to A$). Roman numbers refer to separately scaling the strength of contributions from: (I) and (II) - complex-complex van der Waals and electrostatic interaction (dissociation), (III-V) correspond to the interaction of complexes with solvent via van der Waals forces (III) and separate contributions to electrostatic interactions from Zn ions and the atoms of the salphen units (IV) and phenyl side-groups (V)

accidental loss of contacts between part of aromatic pairs or switch between cation-π and $\pi-\pi$ bonding. To reduce the effect of disconnected fragments, only the simulations where enough contact was maintained ($\Delta G\leq -3$ kcal/mol) were included when calculating averages. Nevertheless, these results are in good qualitative agreement with earlier experimental observations.[30]

Bending elasticity of multiple-chain fibres

It follows from the simulations above that as DCM evaporates it leaves extended Zn-O bonded chains which subsequently link together via phenyl side-groups forming micro-scale fibres with increased rigidity. If such fibres are long enough they are able to form ring-like structures, the diameter of which is comparable[65] to the fibre's persistence length (l_p) - the distance along the chain below which its behaviour can be approximated by the deflection of an elastic rod.[66] The detailed study of such multi-chain fibre structures, assembly rate and elastic behaviour requires millisecond-long simulations of hundreds of periodic units, which is out of the reach of all-atom MD simulations and beyond the scope of this article. However, if the deformation of a fibre under loading follows the continuum mechanics theory (as opposed to entropic elasticity, where deformation is dominated by fluctuations and local conformational changes),[61,67] its persistence length can be related to the bending stiffness of the fibre (B):

$$l_p = \frac{B}{k_B T} \tag{3}$$

where T is the temperature and k_B is the Boltzmann constant.

By analogy with the aforementioned protein sheet-like structures,[59,60] we noticed that a $\pi-\pi$ stacked layer of bis-Zn(salphen) chains can be rolled to form a tubular structure as shown in the figures 7a-c. There clearly can exist entire family of such tubes with different sizes and chiral angles (the angles between the tube axis and the direction of the Zn-O bonded chains) and we do not attempt here to cover all these possible structures. Since the aim of the current work is merely to demonstrate the possibility of bis-Zn(salphen) complexes to assemble into fibres with enough stiffness to form mircoscale rings and rods, here we only studied the particular case of the patch with $m=5$ and $n=4$ (15360 atoms in total), for which the symmetry plane of the layer (the plane formed by $\vec{a}'$ and $\vec{b}'$ vectors and passing through the centre of mass) is rolled around the $(1,-1)$ axis into a cylinder of 3 nm in diameter. In our preliminary calculations, we have found that for such an arrangement the conformation of Zn(salphen) dimers and the structure of $\pi-\pi$ links between the chains remain stable over the course of the simulations. The higher curvature introduces significant stress leading to packing defects causing large discrepancies between different samples, while the tubes with chiral angles close to 0° or 90° are unstable under transversal load, which is essential for the approach used here.

Following prevoius works,[61,67] we have estimated the bending stiffness of such fibres applying a force varying from 16 to 295 pN to the centre of mass of the rightmost section, while the non-hydrogen atoms of the salphen units of the leftmost section were kept frozen after initial relaxation. The direction of the force was chosen to be always perpendicular to the tube axis to avoid longitudinal component, stretching and weakening the structure of the fibre. Such setup represents a cantilever under the action of a constant moment, deflection of which is described in elastic

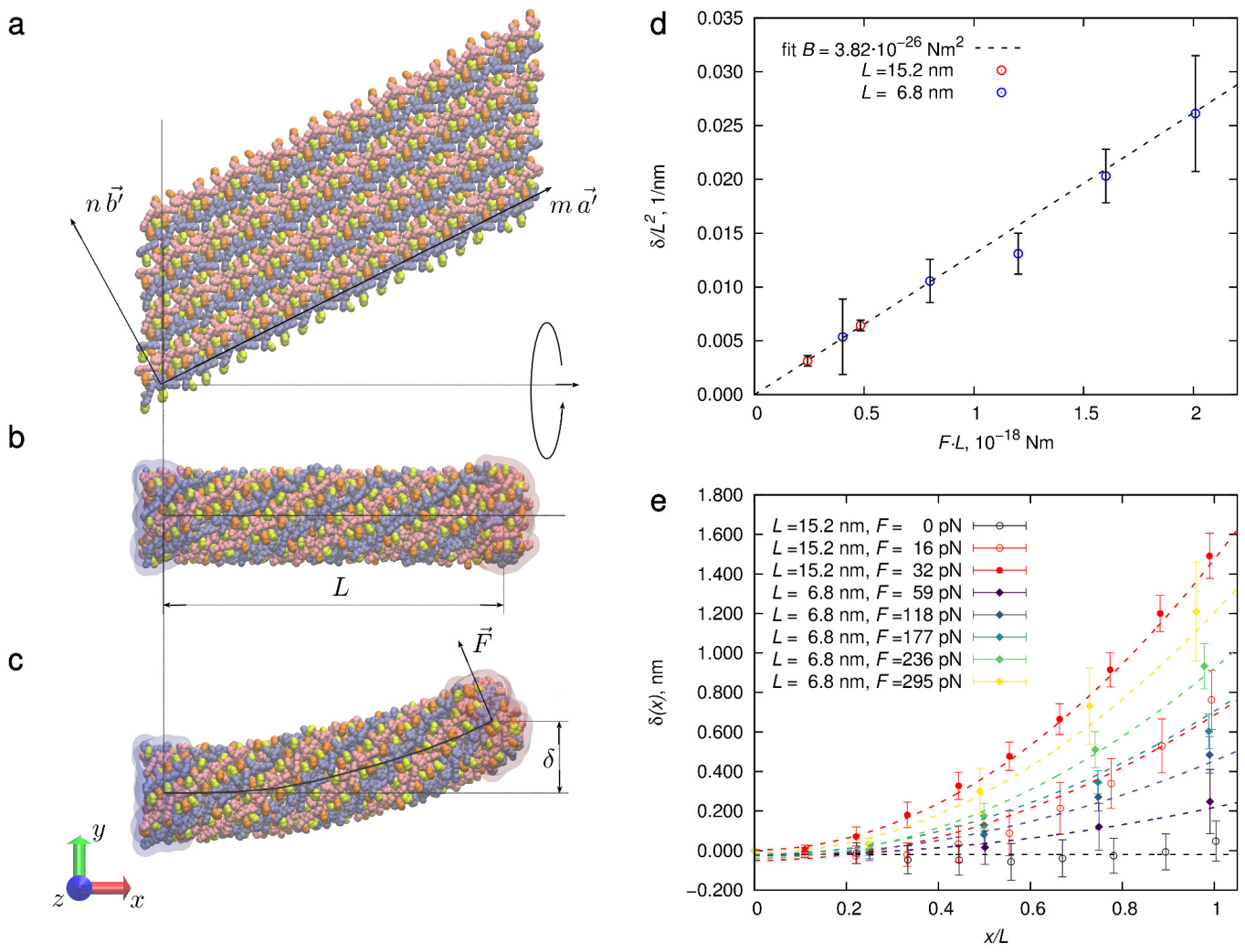

Fig. 7 Structure and bending of a tubular multi-chain fibre: geometry of an unrolled patch of bis-Zn(salphen) 2D layer (a) and the corresponding fibre in a relaxed state (b) and loaded with force F applied to the rightmost section (shaded in pink), while its leftmost section is kept fixed (shaded in blue); $\vec{a'}$ and $\vec{b'}$ are the lattice vectors of the planar layer as described earlier in figure 4c and Table 1; (d) - measured ratio of endpoint deviation δ to squared length L of the fibre against the applied moment $F \cdot L$ and a linear trend (equation (4)) corresponding to the averaged value of bending modulus B; (e) - profile of the loaded fibres: circles indicate the averaged positions of one dimer wide cylindrical sections, while error-bars show their root mean square deviations, dashed lines show the profiles expected for uniform cantilever with the estimated bending modulus

theory by the equation:[68]

$$\delta(x) = \frac{F \cdot L}{2B} x^2 \tag{4}$$

where x - is the coordinate along the initial tube axis and L is the distance between centres of mass of the fixed (leftmost) and loaded (rightmost) sections. These simulations were conducted for the two length values: 6.8 and 15.2 nm, corresponding to 5 and 10 cylindrical sections of one dimer thick (i.e. half-length of the rolled (5,4) patch and its full size). Initial structures were prepared by rolling down the tube of the desired length from a 2D layer with idealized geometry and relaxed during 10 ns, after which the tube axis was aligned to the OX axis. Here O represents the centre of leftmost cylindrical section. The force F, uniformly distributed between the heavy atoms of salphen bases of the rightmost section, was gradually increased up to the desired value during a 2 ns interval. After the desired load was achieved, the behaviour of the tubes was simulated during a time at least 25 ns for the shortest length and up to 40 ns for the longest one until the deflection δ of rightmost section centre of mass was oscillating around a fixed value during at least a 5 ns interval. The final deflections were estimated by averaging during this last 5 ns interval across three independent trajectories for the same value of load, but independently obtained initial structure. From this deflection the bending stiffness modulus was estimated according to the equation (4) with $x = L$:

$$B = \frac{FL^3}{2\delta}. \tag{5}$$

The results of the simulations for different length and loads agree well with the linear trend $\delta/L^2 = F \cdot L/(2B)$ as predicted by continuum theory (figure 7d). The final estimate of bending stiffness of the fibre with the selected structure was determined as the average of the values obtained across all sets of simulations,

and was found to be $B = (3.82 \pm 0.6) \cdot 10^{-26}\,\mathrm{Nm}^2$. Furthermore, the averaged positions of the centres of mass of the one-dimer thick cylindrical belt sections along the fibres were compared to the trend predicted by equation (4) for the estimated value of bending stiffness. As can be seen from the figure 7e the behaviour of the fibre under study agrees well with the predictions of the continuum mechanics theory. This means that the fibre length used in these simulations is well below the persistence length,[61] which in this case can be estimated from equation (3) as $l_P \sim 9.2 \pm 1.4\,\mu\mathrm{m}$ for $T = 298.15\,\mathrm{K}$. The estimates of B and l_P obtained here are comparable to the values determined using a similar approach for protein fibrils,[61] which were found to be in good agreement with known experimental values.

It is important to note that the simulations presented here are performed in vacuum and not in solution. As it was shown earlier using FEP calculations, DCM, the only solvent of interest for this study, decreases the stability of binding of Zn(salphen) chains via phenyl functional groups, promoting their longitudinal growth via Zn-O bonds and letting the chains to achieve micrometre-scale length. So, their agglomeration into elastic fibres is expected to occur not in a well diluted system, but during the solvent evaporation. Clearly the fibres assembled under such non-equilibrium conditions will have many packing defects and, hence, will be more flexible, compared to the idealized case studied here. However, these results prove that high stiffness values can be achieved for the bis-Zn(salphen) chains of the proposed structure already at a very small scale: just 8 chains stacked into a fibre of $\sim 3\,\mathrm{nm}$ in diameter, compared to the experimentally observed thickness of rings and rods of $\sim 100\,\mathrm{nm}$. This observation supports the proposed hypothesis that condensation of long bis-Zn(salphen) chains functionalized with phenyl groups results into fibres with persistence length in the order of micrometres, which will form straight rods or micrometre-sized rings rather than spherical globule.

Conclusion

As discussed in the introduction, the peculiar self-assembly behaviour of phenyl-functionalized bis-Zn(salphen) complexes, synthesized earlier by Escárcega-Bobadilla *et al.* cannot be fully described by vesicle collapse and piercing or other mechanisms which usually result in the emergence of nanorings in self-assembling systems. Instead, based on the detailed molecular-level computer simulations presented here, we suggest that if the molecular structure of bis-Zn(salphen) complex adopts a different conformation from the one previously proposed,[30] it can form stable dimers which link together via pairs of Zn-O bonds into 1D polymeric chains. These chains maintain significant flexibility while remaining single-stranded due to a wide angle of rotation around the central C-C bond of the bis-salphen ligands. However, joining several such chains via phenyl side-groups constrains their movement introducing elastic behaviour.

From our free energy calculations we can also conclude that the growth of such assemblies is strongly dependent on the solvent used. Specifically, the binding free energy of single-stranded chains via $\pi - \pi$ interaction is much smaller in DCM, therefore this solvent promotes formation of longer Zn-O bonded chains, which remain flexible and mobile and, therefore, reach and entangle with other chains. Their aggregation into thicker fibres is only expected to occur at the late stages of solvent evaporation, when the concentration of entangled chains is high enough, most likely in a thinning evaporating film or at the liquid-air or liquid-surface interfaces.

Our estimation of bending stiffness of an idealized 8-chain tubular fibre suggests that, upon evaporation of solvent, such supramolecular fibres should undergo transitions from dissolved coil to rod-like or toroidal globules (figure 8a-c), similar to semi-flexible polymers. The dimensions of such globules are estimated to be in the order of micrometres, which coincides with the observed radius of the self-assembled rings. Such behaviour was routinely observed both experimentally and numerically for certain polymers.[26,69] The key difference here is that, unlike the majority of polymers for which this phenomenon was intensively studied before, the coils, assembling from dimers of bis-Zn(salphen) complexes across wide region of space, are able to bind with each other via the same interactions that bind bis-Zn(salphen) complexes in a coil. This enables the formation of extended "rings-and-rods" webs rather then isolated rings.

Within this mechanism it is possible to explain in a simple and clear way all experimentally observed effects of functional groups and solvent on the ability of such compounds to form networks.[30] While similar-looking structures were noticed even for unsubstituted (i.e. metal-free) ligands, hydrogen-bond mediated formation of similar dimers and chains is less stable than Zn_2O_2 units, thus the structures of unsubstituted ligands were less distinct and disrupted. Replacing the phenyl for a methyl side-group prevents $\pi - \pi$ linking of Zn-O bonded chains into larger and more rigid fibres (figure 8d). Therefore the coils of methyl terminated complexes do not undergo the coil-to-toroidal globule transition, but instead remain in the form of shrinking spherical globules or isolated chains. Strong interactions between the Zn(salphen) units and THF-O atoms slows down longitudinal growth of the chains (figure 8e). So long and flexible chains, vital for the proposed mechanism, do not appear in this solvent. Meanwhile, early association of short Zn-O bonded chains in toluene combined with lower mobility of bis-Zn(salphen) associates and weaker electrostatic screening in this solvent promotes the formation of $\pi - \pi$ bonded 2D sheets and eventually their stacking into nanocrystals (figure 8f).

Naturally, due to computational limitations, the results obtained here with all-atom simulations serve only to clarify the molecular-level picture of the self-assembly process. Macroscale characteristics as solute concentration, solvent evaporation rate, the influence of solvent-substrate and solvent-air interfaces on the particular structure of self-assembled fibres as well as their spatial distribution and the details of their elastic behaviour and plasticity on a larger length and time scale must yet be studied with coarse grained and multiscale approaches, which is out of the scope of the current work.

However, better understanding of the self-assembly process of bis-Zn(salphen) complexes enables synthetic chemists to design other compounds that can exhibit similar behaviour and to experiment with intentional modification of their chemical struc-

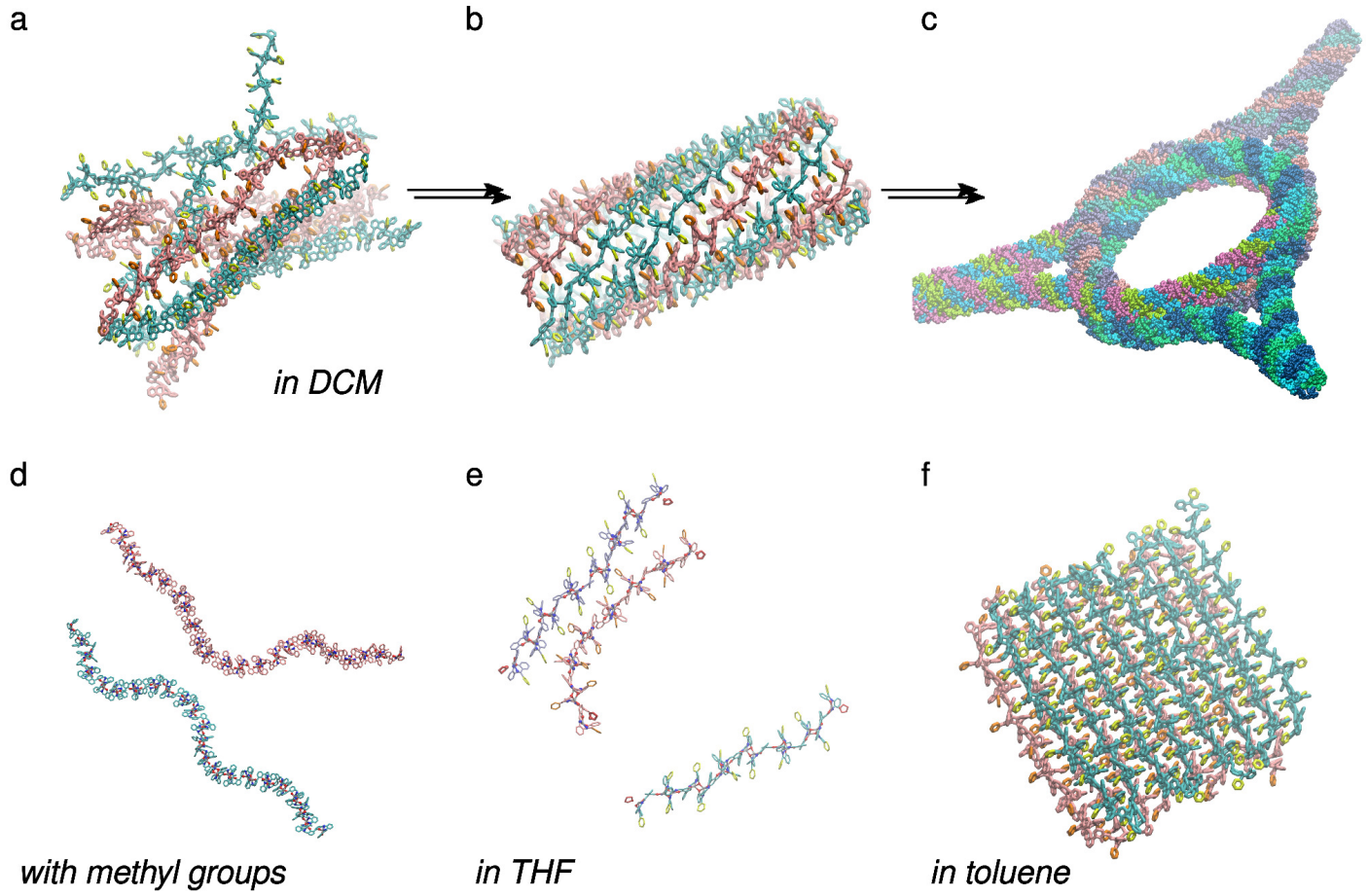

Fig. 8 Expected behaviour of self-assembled chains in the three studied solvents: growth of Zn-O bonded chains in DCM (a), their concatenation via $\pi-\pi$ bonding into extended semiflexible fibres upon solvent evaporation (b) and their consequent co-condensation into rings with multiple outgoing rods, formed by three entangled loops (c); substitution of functional groups with methyl groups leaves single-stranded flexible chains lacking the ability to form rigid fibres through side-chain interactions (d); strong interaction between the THF-O atoms and the Zn cations block the growth of Zn-O bonded chains in THF (e); poor solubility in toluene promotes rapid aggregation of short chains into planar sheets and, ultimately, into layered nanocrystals (f)

tures according to the desired macroscale changes. Furthermore, at a larger scale, folding of a semiflexible polymer chains into a ring and even collection of rings on a string has already been successfully demonstrated using a worm-like chain model (WLC),[21,23,70] free of atomic-level details. Within the proposed mechanism, networks of "rings-and-rods" represent an entirely new level of such phenomena, achieved due to the use of self-assembling supramolecular polymer instead of previously studied chains of fixed length. Therefore it becomes possible to adapt the approaches, such as WLC, developed earlier to study the folding of DNA globules and other polymeric systems to investigate evolution of the morphology of networks from bis-Zn(salphen) complexes and similar compounds.

Such engineered self-assembled webs, capable of patterned deposition and alignment of nanoscale objects, will provide a useful tool for design of novel coatings and bulk materials with programmable properties. Specifically, as our Monte Carlo simulations show,[71] such self-assembled networks used as directing agents for carbon nanotubes have the potential to achieve extremely low values of the percolation thresholds. This makes them highly desirable in such applications as polymer composites[72,73] and transparent electrodes,[74] for which CNTs still have not met initial expectations,[75,76] even when other directing agents, such as worm-like micelles were used.[6]

Methods

Force field parametrization

All molecular dynamics simulations were conducted using LAMMPS software package.[77] All covalent and van der Waals interactions, were parametrised using generalised AMBER force field (GAFF),[78] except of zinc-ligand coordination interactions, which were modelled using "free cation" approach[79] to facilitate formation and breaking for Zn-O bonds during simulation of self-assembly/dissociation of Zn(salphen) supramolecular structures. The force-field parameters were assigned using ANTECHAMBER program from the AmberTools package[80] and MOLTEMPLATE package[81] to create the input files. All bonds with hydrogen atoms were constrained after the initial relaxation stage by the SHAKE algorithm[82] to allow an increased time step of 2.0 fs. The "particle-particle particle-mesh" algorithm (PPPM)[83] was used to treat long range Coulombic interactions. A cutoff radius of 12 Å

was used for van der Waals and short-range electrostatic potentials. Van der Waals interactions were modelled using Lennard-Jones 6-12 potential with a switching function to smooth down the potential profile between 10 and 12 Å as proposed in Ref. 84.

Partial atomic charges were fitted to abinitial electrostatic potential calculated with GAUSSIAN software[85] according to RESP method using Red Tools software package.[86] For this purpose atomic charges an electrostatic potential map for each molecule was calculated using the standard 6-31g* (5d) orbital basis and Hartree-Fock exchange for its geometry, optimised using hybrid Becke 3 parameter Lee-Yang-Parr (B3LYP) functional for exchange and correlation energy .[87,88] The potential values were sampled according to the Merz-Singh-Kollman scheme.[89]

Validation with *ab initio* calculations

To verify the chosen parametrization geometries of several Zn(salphen) complexes, their dimers and interaction potentials were compared against *ab initio* calculations carried out with ONETEP Linear-Scaling DFT package,[90,91] capable of very accurate force calculation.[92] To obtain the initial relaxed coordinates of single bis-Zn(salphen) complexes and their dimers in vacuum the structures derived from X-ray resolved reference geometries in Ref. 30 were first preoptimised with the SIESTA code[93] and subsequently optimised using ONETEP Linear-Scaling DFT package. The plain-wave cutoff for optimisation with ONETEP was set to 1000 eV. NGWF radii were set to 8 Bohr. Norm-conserving pseudopotentials generated with OPIUM package.[94] Exchange and correlation functional was composed of Perdew-Wang form of the local density approximation (LDA) for correlation,[95] combined with Becke exchange.[96] Van der Waals interactions were included into DFT calculations using the approach by Grimme.[97] Iterative self-consistent calculations were conducted until energy convergence below 50 meV and maximum forces below 50 meV/Å per atom for single molecule and 100 meV/Å per atom for molecular dimer were achieved. The results of these calculations can be found in the section S4 of Supplementary Information.

Molecular dynamics simulation protocol

For simulations in vacuum temperature of bis-Zn(salphen) complexes was controlled using Langevin thermostat[62] with 0.1 ps damping parameter. Temperature and pressure of explicit solvent was set to 298.15 K and 1 atm. correspondingly by Nose-Hoover thermostat and barostat (in explicit solvent) with dumping parameters of 0.1 ps for the former and 1.0 ps for the latter. The compound molecules were submerged into cubic boxes with ~900-1000 solvent molecules initially obtained from VirtualChemistry online database[98] equilibrated under periodic conditions (side length 48.1 Å for DCM, 51.2 Å for THF and 56.3 Å for toluene and twice that in one direction for the longest 8-molecular chains). To remove the initial stress while keeping the solute structure close to initial, each simulation started with a relaxation procedure similar to described in Ref. 99. At this stage the atoms of the complexes were restrained to their initial positions with virtual strings, the strength of which decreased exponentially from 600 to 1 kcal/mol/Å during a set of 4-10 intervals 50 ps long, depending on the number of solute molecules, with a timestep of 0.5 fs. Additional virtual springs with the spring constant 5.0 kcal/mol/Å were attached to prevent non-covalently interacting oxygen atoms and metal cations of adjacent complexes from moving initially too far apart during another 100 ps. The stability of the conformations and associations of the bis-Zn(salphen) complexes in explicit solvent was studied by performing 1-5 nanosecond long equilibration runs during which the conformation of the single complex or assembly as well as the change of complex-to-complex and complex-to-solvent interaction energies were monitored. Instantaneous thermodynamics quantities were sampled every 100 timesteps. Every 1000 time steps (or 2 ps) averages over the last 20 samples were collected. The observed values typically converged after the first 0.5-1.0 ns after the relaxation procedure. Diffusion rate was estimated by averaging mean square displacement of a solute[57] during 1 ns over a set of 40 trajectories, among which both "closed" and "open" conformations were equally represented. Statistical deviation was estimated by one-off strategy as described in Ref. 57.

Conformational studies

Conformational space of a stand-alone bis-Zn(salphen) complex in vacuum was studied using the Umbrella Sampling method (US):[55] a restraining potential of quadratic form $U_k = K(\zeta - \zeta_k)^2$ was used for US calculations, where $K = 128\,\mathrm{kcal/mol/Å^2}$ is the spring constant, ζ is the reaction coordinate to be constrained and ζ_k is the value of that coordinate around which the molecular behaviour is studied. For each value of ζ_k 8-16 simulations in vacuum were performed, each starting from a different initial structure, selected from a preceding "nudged elastic band" method[100] simulation of the transition from one configuration to another. Each US simulation consisted of the two parts: during the first 500 ps the system was driven to the target value of the reaction coordinate by gradual changing the position of the minimum of the biasing potential from the initial to the target value. During the consequent 500 ps, the value of the reaction coordinate was sampled every 500 timesteps (or 0.25 ps) while the spring constant was kept at its final value. The weighted histogram analysis (WHAM) of the collected data was performed using the utility with the same name by Alan Grossfield[101] to extract the potentials of mean force in vacuum.

Free energy calculations

During free energy perturbation calculations non-bonding interactions were modelled with "soft-core" versions of the Lennard-Jones and Coulomb potentials[102] as implemented in LAMMPS. The recommended values of 0.5 and 10 $Å^2$ were used for the shape parameters of the potentials correspondingly. The strength of solute-solvent interactions was varied with so-called coupling parameter λ. For better stability van der Waals and Coulomb interactions were scaled separately as proposed in Ref. 103. As in alchemical transformation approach solute is decoupled from solvent, the temperature of the former was controlled separately by a Langevin thermostat.

Free energy changes during FEP calculations were estimated

according to Bennet Acceptance Ratio method.[104] To estimate the solvation free energies perturbations of potential energy in both forward ($\delta U_{FWD}(\lambda_i) = U(\lambda_{i+i}) - U(\lambda_i)$) and backward ($\delta U_{BWD}(\lambda_i) = U(\lambda_{i-i}) - U(\lambda_i)$) directions were accumulated for a set of 71 consequent 600 ps simulations with decreasing values of λ, resulting in 42.6 ns long run for each of independent simulation. Out of this number Coulomb interactions were gradually decoupled during the first 20 points, van der Waals interactions between solvent and phenyl side-groups - during the next 20 points and between solvent and the rest of the complex - during the last 31. All interactions were scaled down linearly. For each λ-point the first 400 ps were used for equilibration and the last 200 - for data collection. A similar approach was used for dissociation free energy in vacuum. This time, however, each λ-point was equal to 300 ps resulting in 21.3 ns long runs. The λ-schedule for dissociation procedure consisted of 35 points for Coulomb interactions, followed by 36 for the van der Waals attraction, separated from repulsion with Weeks-Chandler-Andersen decomposition.[105] The change of the free energy, corresponding to each transition ($\lambda_i \rightarrow \lambda_{i+1}$), was estimated using Bennett acceptance ratio method (BAR) as implemented in the ParseFEP plugin to VMD.[106]

Acknowledgements

The research leading to these results was funded by European Community's Seventh Framework Program through Marie Curie Initial Training Network "CONTACT" (FP7-PEOPLE-ITN2008-238363) and Portuguese Foundation of Science and Technology (FCT) through the PhD grant SFRH/BD/ 88995/2012. The Center of Physics of University of Minho research is sponsored by FCT in the framework of the Strategic Funding UID/FIS/04650/2013. The authors also acknowledge the support of the Winton Programme for the Physics of Sustainability and of the Spanish Ministerio de Economï¿œa y Competitividad (MINECO, project CTQ-201460419-R). Computer facilities were provided by the "Search-ON2: Revitalization of HPC infrastructure of UMinho" (NORTE-07-0162-FEDER-000086), co-funded by the North Portugal Regional Operational Programme (ON.2 – O Novo Norte), under the National Strategic Reference Framework (NSRF), through the European Regional Development Fund (ERDF).

Notes and references

1 V. Blasjo, *Am. Math. Mon.*, 2005, **112**, 526–566.
2 A. Shimoni, S. Azoubel and S. Magdassi, *Nanoscale*, 2014, **6**, 11084–11089.
3 M. Mohl, A. Dombovari, R. Vajtai, P. M. Ajayan and K. Kordas, *Sci. Rep.*, 2015, **5**, 13710.
4 W. Zhou, J. Chen, Y. Li, D. Wang, J. Chen, X. Feng, Z. Huang, R. Liu, X. Lin, H. Zhang, B. Mi and Y. Ma, *ACS Appl. Mater. Interfaces*, 2016, **8**, 11122–11127.
5 J. Xie, H. Wang, H. Bai, P. Yang, M. Shi, P. Guo, C. Wang, W. Yang and H. Song, *ACS Appl. Mater. Interfaces*, 2012, **4**, 2891–2896.
6 J. J. Cardiel, Y. Zhao, J.-H. Kim, J.-H. Chung and A. Q. Shen, *Carbon*, 2014, **80**, 203–212.
7 M. C. Lensen, K. Takazawa, J. A. A. W. Elemans, C. R. L. P. N. Jeukens, P. C. M. Christianen, J. C. Maan, A. E. Rowan and R. J. M. Nolte, *Chem.–Eur. J.*, 2004, **10**, 831–839.
8 K. Takazawa, *Chem. Mater.*, 2007, **19**, 5293–5301.
9 Y. Liu, H. Ma, Y. Tian, F. Xie and X. Wang, *Macromol. Chem. Phys.*, 2014, **215**, 1446–1455.
10 Y. Kang, K. Liu and X. Zhang, *Langmuir*, 2014, **30**, 5989–6001.
11 Z. Chu, C. a. Dreiss and Y. Feng, *Chem. Soc. Rev.*, 2013, **42**, 7174.
12 Y. Feng and Z. Chu, *Soft Matter*, 2015, **11**, 4614–4620.
13 Y. Li, H. Li, J. Chai, M. Chen, Q. Yang and J. Hao, *Langmuir*, 2015, **31**, 11209–11219.
14 H. Lu, Q. Shi, B. Wang and Z. Huang, *Colloids Surf., A*, 2016, **494**, 74–80.
15 H. Cui, Z. Chen, K. L. Wooley and D. J. Pochan, *Soft Matter*, 2009, **5**, 1269–1278.
16 S. J. Holder and N. a. J. M. Sommerdijk, *Polym. Chem.*, 2011, **2**, 1018.
17 D. J. Pochan, *Science*, 2004, **306**, 94–97.
18 H. Yu and W. Jiang, *Macromolecules*, 2009, **42**, 3399–3404.
19 V. M. Suresh, S. J. George and T. K. Maji, *Adv. Funct. Mater.*, 2013, **23**, 5585–5590.
20 T. X. Hoang, A. Giacometti, R. Podgornik, N. T. T. Nguyen, J. R. Banavar and A. Maritan, *J. Chem. Phys.*, 2014, **140**, 064902.
21 Y.-F. Wei and P.-Y. Hsiao, *J. Chem. Phys.*, 2007, **127**, 064901.
22 T. Iwaki, N. Makita and K. Yoshikawa, *J. Chem. Phys.*, 2008, **129**, 065103.
23 Z. Ou and M. Muthukumar, *J. Chem. Phys.*, 2005, **123**, 074905(9).
24 V. A. Markov, V. V. Vasilevskaya, P. G. Khalatur, G. ten Brinke and A. R. Khokhlov, *Polym. Sci. Ser. A*, 2008, **50**, 621–629.
25 S. Danielsen, K. M. Vårum and B. T. Stokke, *Biomacromolecules*, 2004, **5**, 928–936.
26 G. Maurstad and B. T. Stokke, *Biopolymers*, 2004, **74**, 199–213.
27 a solvent with lower value of the second virial coefficient,[?] which leads to contraction of globules[?] .
28 T. Sakaue and K. Yoshikawa, *J. Chem. Phys.*, 2006, **125**, 074904.
29 A. Lappala and E. M. Terentjev, *Macromolecules*, 2013, **46**, 7125–7131.
30 M. V. Escárcega-Bobadilla, G. a. Zelada-Guillén, S. V. Pyrlin, M. Wegrzyn, M. M. Ramos, E. Giménez, A. Stewart, G. Maier and A. W. Kleij, *Nat. Commun.*, 2013, **4**, 2648.
31 A. I. Victorov, M. A. Voznesenskiy and E. A. Safonova, *Russ. Chem. Rev.*, 2015, **84**, 693–711.
32 F. Dutertre, C. Gaillard, C. Chassenieux and T. Nicolai, *Macromolecules*, 2015, **48**, 7604–7612.
33 A. W. Kleij, *Dalton Trans.*, 2009, 4635.
34 Y.-B. Cai, J. Zhan, Y. Hai and J.-L. Zhang, *Chemistry*, 2012, **18**, 4242–9.
35 D. Anselmo, G. Salassa, E. C. Escudero-Adán, E. Martin and

A. W. Kleij, *Dalton Trans.*, 2013, **42**, 7962.
36 G. Consiglio, S. Failla, C. G. Fortuna, L. D'Urso and G. Forte, *Comput. Theor. Chem.*, 2015, **1067**, 1–6.
37 G. Consiglio, S. Failla, I. P. Oliveri, R. Purrello and S. Di Bella, *Dalton Trans.*, 2009, 10426.
38 I. P. Oliveri, G. Malandrino and S. Di Bella, *Inorg. Chem.*, 2014, **53**, 9771–9777.
39 N. Kielland, E. C. Escudero-Adán, M. Martínez Belmonte and A. W. Kleij, *Dalton Trans.*, 2013, **42**, 1427–1436.
40 J. Janczak, D. Prochowicz, J. Lewiński, D. Fairen-Jimenez, T. Bereta and J. Lisowski, *Chem. Eur. J.*, 2016, **22**, 598–609.
41 O. Shoji, H. Tanaka, T. Kawai and Y. Kobuke, *J. Am. Chem. Soc.*, 2005, **127**, 8598–8599.
42 G. Salassa, M. J. J. Coenen, S. J. Wezenberg, B. L. M. Hendriksen, S. Speller, J. a. a. W. Elemans and A. W. Kleij, *J. Am. Chem. Soc.*, 2012, **134**, 7186–7192.
43 M. Piccinno, C. A. Angulo-Pachón, P. Ballester, B. Escuder and A. D. Cort, *RSC Adv.*, 2016, **6**, 57306–57309.
44 J. K.-H. Hui, Z. Yu and M. J. MacLachlan, *Angew. Chem. Int. Ed.*, 2007, **46**, 7980–7983.
45 I. P. Oliveri, G. Malandrino and S. Di Bella, *Dalton Trans.*, 2014, **43**, 10208.
46 R. Haldar, S. Bonakala, P. Kanoo, S. Balasubramanian and T. K. Maji, *CrystEngComm*, 2014, **16**, 4877.
47 S. Curreli, E. C. Escudero-Adán, J. Benet-Buchholz and A. W. Kleij, *Eur. J. Inorg. Chem.*, 2008, **2008**, 2863–2873.
48 M. Viciano-Chumillas, D. Li, A. Smogunov, S. Latil, Y. J. Dappe, C. Barreteau, T. Mallah and F. Silly, *Chem.–Eur. J.*, 2014, **20**, 13566–13575.
49 J. Wang, W. Huang, L. Pan, H. Wang, C. Zhang and X. Liu, *Macromol. Res.*, 2015, **23**, 309–312.
50 A. M. Castilla, S. Curreli, N. M. Carretero, E. C. Escudero-Adán, J. Benet-Buchholz and A. W. Kleij, *Eur. J. Inorg. Chem.*, 2009, **2009**, 2467–2471.
51 S. F. Fenz and K. Sengupta, *Integr. Biol.*, 2012, **4**, 982.
52 P. Walde, K. Cosentino, H. Engel and P. Stano, *Chembiochem*, 2010, **11**, 848–865.
53 J. Xiao and J. Du, *Polym. Chem.*, 2016, **7**, 4647–4653.
54 In fact there are two Φ angles - one per each salphen base, however, only one needs to be studied due to molecular symmetry.
55 P. Virnau and M. Muller, *J. Chem. Phys.*, 2004, **120**, 10925.
56 M. Abdellatif, G. Abdelrasoul, A. Scarpellini, S. Marras and A. Diaspro, *J. Colloid Interface Sci.*, 2015, **458**, 266–272.
57 J. Wang and T. Hou, *J. Comput. Chem.*, 2011, **32**, 3505–3519.
58 R. Mangal, S. Srivastava, S. Narayanan and L. A. Archer, *Langmuir*, 2016, **32**, 596–603.
59 A. G. Murzin, A. M. Lesk and C. Chothia, *J. Mol. Biol.*, 1994, **236**, 1369–1381.
60 A. G. Murzin, A. M. Lesk and C. Chothia, *J. Mol. Biol.*, 1994, **236**, 1382–1400.
61 M. Solar and M. J. Buehler, *Nanoscale*, 2012, **4**, 1177–83.
62 R. L. Davidchack, R. Handel and M. V. Tretyakov, *J. Chem. Phys.*, 2009, **130**, 234101.
63 V. A. Ivanov, J. A. Martemyanova, A. S. Rodionova and M. R. Stukan, *Polym. Sci. Ser. C*, 2013, **55**, 4–22.
64 D. Shivakumar, J. Williams, Y. Wu, W. Damm, J. Shelley and W. Sherman, *J. Chem. Theory Comput.*, 2010, **6**, 1509–1519.
65 P. Cifra and T. Bleha, *Macromol. Symp.*, 2010, **296**, 336–341.
66 I. K. Piechocka, K. A. Jansen, C. P. Broedersz, N. A. Kurniawan, F. C. MacKintosh and G. H. Koenderink, *Soft Matter*, 2016, **12**, 2145–2156.
67 L. Ruiz, P. VonAchen, T. D. Lazzara, T. Xu and S. Keten, *Nanotechnology*, 2013, **24**, 195103/1–195103/11, 11 pp.
68 L. Bucciarelli, *Engineering mechanics for structures*, Dover, Mineola, N.Y, 2009, p. 320.
69 G. Pereira, *Curr. Appl Phys.*, 2008, **8**, 347–350.
70 V. a. Ivanov, W. Paul and K. Binder, *J. Chem. Phys.*, 1998, **109**, 5659–5669.
71 S. Pyrlin, *Ph.D. thesis*, University of Minho, 2016.
72 Z. Spitalsky, D. Tasis, K. Papagelis and C. Galiotis, *Prog. Polym. Sci.*, 2010, **35**, 357–401.
73 A. V. Eletskii, A. a. Knizhnik, B. Potapkin and J. Kenny, *Uspekhi Fizicheskih Nauk*, 2015, **185**, 225–270.
74 A. J. Stapleton, S. Yambem, A. H. Johns, C. T. Gibson, C. J. Shearer, A. V. Ellis, J. G. Shapter, G. G. Andersson, J. S. Quinton, P. L. Burn, P. Meredith and D. A. Lewis, *J. Mater. Chem. A*, 2015, **3**, 13892–13899.
75 H.-S. Jangr, S. K. Jeon, D. S. Shim, N. H. Lee and S. H. Nahm, *J. Nanosci. Nanotechnol.*, 2015, **15**, 9071–9076.
76 H. D. Yun, J. Kwak, S.-Y. Kim, H. Seo, I. C. Bang, S. Y. Kim, S. Kang and S.-Y. Kwon, *J. Alloys Compd.*, 2016, **675**, 37–45.
77 S. Plimpton, *J. Comput. Phys.*, 1995, **117**, 1–19.
78 J. Wang, R. M. Wolf, J. W. Caldwell, P. A. Kollman and D. A. Case, *J. Comput. Chem.*, 2004, **25**, 1157–1174.
79 R. H. Stote and M. Karplus, *Protein Struct. Funct. Genet.*, 1995, **23**, 12–31.
80 J. Wang, W. Wang, P. A. Kollman and D. A. Case, *J. Mol. Graphics Modell.*, 2006, **25**, 247–260.
81 *Moltemplate*, http://www.moltemplate.org/.
82 J.-P. Ryckaert, G. Ciccotti and H. J. Berendsen, *J. Comput. Phys.*, 1977, **23**, 327–341.
83 B. A. Luty, M. E. Davis, I. G. Tironi and W. F. Van Gunsteren, *Mol. Simul.*, 1994, **14**, 11–20.
84 J. Norberg and L. Nilsson, *Biophys. J.*, 2000, **79**, 1537–1553.
85 M. J. Frisch, G. W. Trucks, H. B. Schlegel, G. E. Scuseria, M. A. Robb, J. R. Cheeseman, J. A. Montgomery, Jr., T. Vreven, K. N. Kudin, J. C. Burant, J. M. Millam, S. S. Iyengar, J. Tomasi, V. Barone, B. Mennucci, M. Cossi, G. Scalmani, N. Rega, G. A. Petersson, H. Nakatsuji, M. Hada, M. Ehara, K. Toyota, R. Fukuda, J. Hasegawa, M. Ishida, T. Nakajima, Y. Honda, O. Kitao, H. Nakai, M. Klene, X. Li, J. E. Knox, H. P. Hratchian, J. B. Cross, V. Bakken, C. Adamo, J. Jaramillo, R. Gomperts, R. E. Stratmann, O. Yazyev, A. J. Austin, R. Cammi, C. Pomelli, J. W. Ochterski, P. Y. Ayala, K. Morokuma, G. A. Voth, P. Salvador, J. J. Dannenberg,

V. G. Zakrzewski, S. Dapprich, A. D. Daniels, M. C. Strain, O. Farkas, D. K. Malick, A. D. Rabuck, K. Raghavachari, J. B. Foresman, J. V. Ortiz, Q. Cui, A. G. Baboul, S. Clifford, J. Cioslowski, B. B. Stefanov, G. Liu, A. Liashenko, P. Piskorz, I. Komaromi, R. L. Martin, D. J. Fox, T. Keith, M. A. Al-Laham, C. Y. Peng, A. Nanayakkara, M. Challacombe, P. M. W. Gill, B. Johnson, W. Chen, M. W. Wong, C. Gonzalez and J. A. Pople, *J. Comput. Chem.*, 2004, **24**, 1748–57.

86 F.-Y. Dupradeau, A. Pigache, T. Zaffran, C. Savineau, R. Lelong, N. Grivel, D. Lelong, W. Rosanski and P. Cieplak, *Phys. Chem. Chem. Phys.*, 2010, **12**, 7821.

87 C. Lee, W. Yang and R. G. Parr, *Phys. Rev. B*, 1988, **37**, 785–789.

88 A. D. Becke, *J. Chem. Phys.*, 1993, **98**, 5648.

89 U. C. Singh and P. A. Kollman, *J. Comput. Chem.*, 1984, **5**, 129–145.

90 C.-K. Skylaris, P. D. Haynes, A. A. Mostofi and M. C. Payne, *J. Chem. Phys.*, 2005, **122**, 084119.

91 K. A. Wilkinson, N. D. M. Hine and C.-K. Skylaris, *J. Chem. Theory Comput.*, 2014, **10**, 4782–4794.

92 N. D. M. Hine, M. Robinson, P. D. Haynes, C.-K. Skylaris, M. C. Payne and A. A. Mostofi, *Phys. Rev. B*, 2011, **83**, 195102.

93 J. M. Soler, E. Artacho, J. D. Gale, A. García, J. Junquera, P. Ordejón and D. Sánchez-Portal, *J. Phys.: Condens. Matter*, 2002, **14**, 2745–2779.

94 *OPIUM pseudopotential generation package*, http://opium.sourceforge.net/.

95 J. P. Perdew and Y. Wang, *Phys. Rev. B*, 1992, **45**, 13244–13249.

96 A. D. Becke, *Phys. Rev. A*, 1988, **38**, 3098–3100.

97 S. Grimme, *J. Comput. Chem.*, 2006, **27**, 1787–1799.

98 *VirtualChemistry.org*, http://virtualchemistry.org/.

99 L. Ruiz and S. Keten, *J. Eng. Mech.*, 2014, **140**, 431–442.

100 G. Henkelman, B. P. Uberuaga and H. Jonsson, *J. Chem. Phys.*, 2000, **113**, 9901.

101 A. Grossfield, *WHAM: the weighted histogram analysis method*, http://membrane.urmc.rochester.edu/content/wham.

102 T. C. Beutler, A. E. Mark, R. C. van Schaik, P. R. Gerber and W. F. van Gunsteren, *Chem. Phys. Lett.*, 1994, **222**, 529–539.

103 Y. Deng and B. Roux, *J. Phys. Chem. B*, 2004, **108**, 16567–16576.

104 C. H. Bennett, *J. Comput. Phys.*, 1976, **22**, 245–268.

105 J. D. Weeks, *Chin. J. Chem. Phys.*, 1971, **54**, 5237.

106 P. Liu, F. Dehez, W. Cai and C. Chipot, *J. Chem. Theory Comput.*, 2012, **8**, 2606–2616.